Research Square

Preprints are preliminary reports that have not undergone peer review.
They should not be considered conclusive, used to inform clinical practice,
or referenced by the media as validated information.

UCHL1 deubiquitinates and stabilizes SLC25A5 to drive pyrotinib resistance in HER2-positive breast cancer

Xinyuan Ding

aladdine@163.com

the Affiliated Suzhou Municipal Hospital, Nanjing Medical University https://orcid.org/0000-0002-8982-6807

Ying Zhu

The Affiliated Suzhou Hospital of Nanjing Medical University, Suzhou Municipal Hospital

Qian Liu

The Affiliated Suzhou Hospital of Nanjing Medical University, Suzhou Municipal Hospital

Juan Wu

The Affiliated Suzhou Hospital of Nanjing Medical University, Suzhou Municipal Hospital

Jianyu Xu

the Affiliated Suzhou Hospital of Nanjing Medical University, Suzhou, China

Zheng Wang

Department of General Surgery, Comprehensive Breast Health Center, Ruijin Hospital, Shanghai Jiao Tong University School of Medicine https://orcid.org/0000-0003-4519-0795

Renhong Huang

Department of General Surgery, Comprehensive Breast Health Center, Ruijin Hospital, Shanghai Jiao Tong University School of Medicine, Shanghai, China

Minzhe Xu

Suzhou University of Science and Technology

Guangjuan Xu

The Affiliated Suzhou Hospital of Nanjing Medical University, Suzhou Municipal Hospital

YanXia Yu

the Affiliated Suzhou Hospital of Nanjing Medical University

Article

Keywords: HER2-positive breast cancer, pyrotinib, treatment resistance, UCHL1, SLC25A5

Posted Date: October 23rd, 2026

DOI: https://doi.org/10.21203/rs.3.rs-11209085/v1

License: This work is licensed under a Creative Commons Attribution 4.0 International License.
Read Full License

Additional Declarations: (Not answered)

Abstract

Pyrotinib, a novel oral pan-HER tyrosine kinase inhibitor (TKI), is a standard first-line therapy for advanced HER2-positive breast cancer, yet drug resistance limits its clinical utility. By integrating public datasets with our institutional tissue specimens, we analyzed the correlations between UCHL1 expression and overall survival as well as pyrotinib response. UCHL1 was upregulated in HER2-positive breast cancer tissues, and its overexpression was correlated with poor prognosis and pyrotinib resistance. Functionally, UCHL1 overexpression promoted pyrotinib resistance, whereas pharmacological inhibition of UCHL1 with LDN-57444 significantly restored the sensitivity of resistant cells to pyrotinib and doxorubicin. An unbiased proteomic approach identified solute carrier family 25 member 5 (SLC25A5) as a potential novel UCHL1 substrate. Mechanistically, UCHL1 catalyzed K11-linked deubiquitination to stabilize SLC25A5, and then enhanced autophagy and DNA damage repair signaling in tumor cells. In summary, UCHL1 stabilizes SLC25A5 via deubiquitination, thereby modulating autophagy and DDR and consequently conferring pyrotinib resistance in HER2-positive breast cancer. These findings highlight UCHL1 as a promising therapeutic target for overcoming pyrotinib-mediated drug resistance in HER2-positive breast cancer.

INTRODUCTION

Breast cancer ranks as the most frequent malignancy in women globally, and human epidermal growth factor receptor 2 (HER2) amplification occurs in 15%-20% of all breast cancer cases [1]. Available therapeutic strategies for HER2-positive breast cancer primarily involve antibody-drug conjugates and tyrosine kinase inhibitors (TKIs), which are frequently combined with anthracycline-based chemotherapy regimens [2]. Pyrotinib, an oral irreversible pan-HER TKI, in combination with trastuzumab and docetaxel, represents a first-line therapeutic option for advanced HER2-positive breast cancer in Chinese clinical practice [3]. Nevertheless, a substantial proportion of patients develop intrinsic or acquired resistance to pyrotinib-based regimens [4]. The underlying molecular mechanisms and actionable therapeutic targets remain poorly understood [5].

TKI resistance is driven by diverse mechanisms, including oncogene mutations, altered metabolism, autophagy, and DNA damage repair (DDR) [6]. In HER2-positive breast cancer, HER2-TKI treatment triggers autophagy to protect tumor cells [7]. Autophagy facilitates tumor cell survival by eliminating damaged organelles, thereby mediating acquired resistance to targeted therapy [8]. Meanwhile, HER2-TKI induces DNA damage in tumor cells [9]. Excessive activation of the DDR pathway enhances DNA-repair capacity to counteract drug-mediated cytotoxic effects, which also contributes to HER2-targeted resistance [10]. DDR and autophagy converge to drive tumor progression and therapeutic resistance, particularly multidrug resistance in tumors [11]. Therefore, exploring the function of these pathways in TKI-therapy may help explain pyrotinib resistance.

The ubiquitin-proteasome system (UPS) mediates multidrug resistance in breast cancer through ubiquitination-mediated degradation [12]. For instance, TRIM21-mediated ubiquitination of RBM38c

facilitates autophagy in cancer cells [13], while USP25 promotes chemoresistance by enhancing DNA double-strand break repair [14]. In the context of pyrotinib response, pyrotinib promotes GRP78 degradation via K48-linked ubiquitination in gastric cancer [15], also induces ARIH1-dependent HER2 degradation in lung cancer [16], and synergizes with chrysin to induce tumor cell death in HER2-positive breast cancer [7]. Nevertheless, to our knowledge, no ubiquitinating enzymes have been reported to regulate pyrotinib resistance. Ubiquitin C-terminal hydrolase L1 (UCHL1), a neuron-enriched deubiquitinating enzyme [17], and as we have previously demonstrated, drives doxorubicin resistance in HER2-positive breast cancer [18], and also mitigates pemetrexed-induced DNA damage and cell-cycle arrest to confer chemoresistance in lung cancer [19], and stabilizes keratin 8 to promote temozolomide resistance in glioblastoma [20]. However, whether UCHL1 modulates pyrotinib resistance and its underlying mechanisms remains unclear.

Here, we demonstrate that the high expression of UCHL1 is positively correlated with pyrotinib resistance in HER2-positive breast cancer. Inhibition of UCHL1 increases tumor cell sensitivity to pyrotinib and doxorubicin both *in vitro* and *in vivo*. Mechanistically, UCHL1 enhances protective autophagy and DDR signaling by deubiquitinating K11-linked ubiquitin chains and stabilizing SLC25A5, thereby driving pyrotinib resistance in HER2-positive breast cancer. Collectively, UCHL1 may serve as an effective biomarker and therapeutic target for individualized combination therapy with TKIs and anthracyclines in patients with HER2-positive breast cancer.

MATERIALS AND METHODS

Cell lines and pyrotibib-resistant cells construction

The normal human mammary epithelial cell line MCF-10A, human breast cancer cell line SK-BR-3 and MDA-MB-231 were obtained from the Type Culture Collection of the Chinese Academy of Sciences (Shanghai, China). SUM159 and BT474 were purchased from Procell Biotechnology (Wuhan, Hubei, China). The murine HER2-positive mammary carcinoma cell line TUBO was purchased from Sigma-Aldrich (St. Louis, MO, USA). All cell lines were cultured according to the manufacturer's instructions.

Pyrotinib-resistant SK-BR-3-R cells were generated from parental SK-BR-3 cells via stepwise dose escalation of pyrotinib (Cat# HY-104065, MedChemExpress; Monmouth Junction, New Jersey, USA) over five months. Subsequently, SK-BR-3-R cells were cultivated in the medium containing 500 nM pyrotinib.

Cell transfection and stable cell line generation

The UCHL1 knockdown plasmids and their corresponding negative controls (sequences listed in Table S1), the human *UCHL1* overexpression plasmid (Cat# P89449), and mouse *Uchl1* overexpression plasmid (Cat# P66753) were all obtained from MiaoLing Biotechnology Co., Ltd. (Wuhan, Hubei, China). All plasmids were introduced into cells using the TransIT-X2 Dynamic Delivery System (Cat# MIR6000; Mirus Bio, Madison, USA). For stable cell lines, lentiviral particles were produced by co-transfecting

HEK293T cells with the transfer plasmid, psPAX2 (Cat# 12260, Addgene; Watertown, MA, USA) and pMD2.G (Cat# 12259, Addgene) using the same reagent. The desired cells were infected with viral supernatants in the presence of polybrene (Cat# TR-1003, Sigma-Aldrich) and selected with puromycin (Cat# A1113802, Thermo Fisher Scientific; Waltham, MA, USA).

Quantitative PCR (qPCR)

Total RNA was extracted from cells using RNA-easy Isolation Reagent (Cat# R701-01, Vazyme; Nanjing, Jiangsu, China) according to the manufacturer's instructions. Complementary DNA (cDNA) was synthesized from 1 μg of total RNA using HiScript □ RT SuperMix (Cat# R701, Vazyme). Quantitative PCR was subsequently conducted using Taq Pro Universal SYBR qPCR Master Mix on a Real-Time PCR System. The primer sequences are listed in Table S2.

Western blotting

Western blotting
The detailed experimental procedure has been described in our previous study [18]. Primary antibodies were as follows: from Proteintech (Wuhan, Hubei, China): anti-UCHL1 (Cat# 14730-1-AP), anti-Flag (Cat# 20543-1-AP); from Cell Signaling Technology (Danvers, MA, USA): anti-Myc (Cat# 2276), anti-Beclin 1 (Cat# 3495), anti-p62 (Cat# 39749), anti-LC3 (Cat# 12741); from Abclonal (Wuhan, Hubei, China): anti-GAPDH (Cat# A19056), anti-TOP2A (Cat# A4389), anti-MSH2 (Cat# A8740), anti-SLC25A5 (Cat# A15639SP); and from Abmart (Shanghai, China): anti-γ-H2AX (Ser139) (Cat# M63324), anti-H2AX (Cat# PA1524).

CCK-8 and colony formation assays

The Cell Counting Kit-8 (CCK-8, Cat# CK04, Dojindo; Kumamoto, Japan) assay was performed strictly following the manufacturer's instructions. For colony formation assay, the cells were digested, and then 300 cells per well were seeded into a six-well plate. Following treatment, the plate was incubated at 37°C in a 5% CO_2 environment for two weeks. After incubation, the cells were washed twice with PBS. Subsequently, the cells were stained using a Wright-Giemsa Stain Kit from Jiancheng (Cat# D010-1; Nanjing, Jiangsu, China).

Immunofluorescence staining

Cells were cultured on confocal dishes and fixed with 4% paraformaldehyde for 15 min, followed by PBS washing and permeabilization with 0.1% Triton X-100. After blocking with 1% BSA (Cat# IB9040, Solarbio; Beijing, China), the cells were incubated with primary antibodies at 4°C overnight. The next day, fluorescent secondary antibodies were applied at room temperature for 1 h in the dark. Cell nuclei were

stained with DAPI (Cat# C1006, Beyotime; Shanghai, China), and an anti-fade mounting medium was added before imaging with a Leica Stellaris 5 confocal laser scanning microscope.

Comet assay

Melted agarose was dropped onto a slide, covered with a coverslip, and solidified at 4°C for 15 min to form the first agarose layer. A cell suspension was mixed with preheated agarose, layered onto the first gel, covered, and again solidified at 4°C for 15 min to form the second layer. After coverslip removal, the slides were lysed in precooled lysis buffer at 4°C for 2 h to release DNA. Subsequently, the slides were rinsed with distilled water, equilibrated in electrophoresis buffer for 40 min, and electrophoresed for 30 min. Following electrophoresis, the slides were neutralized and stained for 10 min. Images were captured under a fluorescence microscope [21].

Immunohistochemistry (IHC)

IHC staining was conducted using the commercial kit (Cat# PV-9000, ZSGB-BIO; Beijing, China) following the manufacturer's protocol. The slides were deparaffinized, hydrated, and subjected to antigen retrieval with citric acid solution, then blocked with peroxidase. Then, the slides were incubated with primary antibodies for 24 h. After incubation, diaminobenzidine solution was added according to the manufacturer’s instructions to visualize the antigen-antibody complex. Cell nuclei were stained with hematoxylin. Subsequently, the sections were dehydrated and cleared. Finally, the slides were mounted with resin and photographed under a microscope.

Immunoprecipitation and co-immunoprecipitation

Cell lysates were incubated with the appropriate antibody at 4°C overnight, followed by capture with Dynabeads™ Protein A magnetic beads (Cat# 10002D, Thermo Fisher Scientific). The immunoprecipitated complexes were eluted and separated using sodium dodecyl sulfate-polyacrylamide gel electrophoresis, followed by western blotting with the indicated antibodies. For mass spectrometry, gel in-solution digestion was performed, followed by liquid chromatography-tandem mass spectrometry analysis, with at least two unique peptides were required for reliable protein identification [22].

Syngeneic mouse model

To establish a syngeneic mouse model, 0.5 million TUBO-*UCHL1* cells were orthotopically injected into the mammary fat pad of 6-week-old female *BALB/c* mice (GemPharmatech; Nanjing, Jiangsu, China). Tumor-bearing mice were randomly assigned to different groups and received pyrotinib (10 mg/kg/day) [23] via oral gavage or LDN-57444 (0.4 mg/kg/day, Cat# S7135, Selleck; Houston, TX, USA) [24] via intraperitoneal injection as scheduled. Body weight and tumor volume (calculated as length × width² × 0.5) were monitored. Mice were euthanized when the maximum tumor diameter reached approximately

1500 mm^3. After 21 days, the mice were euthanized, and tumors were excised, weighed, and photographed.

Bioinformatic analysis

GEO datasets (https://www.ncbi.nlm.nih.gov/): GSE132055 (transcriptomes of parental HER2-positive breast cancer cells and derivatives with acquired resistance to anti-HER2 treatments) and GSE62074 (RNA-seq of parental and lapatinib-resistant HCC1419 cells) were analyzed for differential expression [25]. UCHL1 expression levels between response and non-response groups were analyzed using the R2 Genomics Analysis and Visualization Platform (https://hgserver1.amc.nl/cgi-bin/r2/main.cgi), based on the TCGA-BRCA dataset. Drug sensitivity was analyzed using the Gene Set Cancer Analysis (GSCA) portal (https://guolab.wchscu.cn/GSCA/) [26]. Survival curves were systematically evaluated based on Kaplan-Meier plots (https://kmplot.com/) [27]. The UALCAN database (http://ualcan.path.uab.edu/) was employed to analyze SLC25A5 expression profiles across different clinical stages of breast cancer.

Statistical analysis

All analyses were conducted using GraphPad Prism 9. All measurement data are presented as mean ± SEM. At least three independent experiments were conducted per group. Intergroup comparisons for continuous and categorical variables were conducted using two-tailed Student's *t*-test and the χ^2 test or Fisher's exact test, respectively. Differences were considered statistically significant when $P < 0.05$.

RESULTS

Association of UCHL1 expression with pyrotinib resistance in HER2-positive breast cancer

Two GEO datasets, GSE62074 and GSE132055, were used to identify differentially expressed genes (DEGs) involved in therapeutic resistance in HER2-positive breast cancer (Fig. 1A), and *UCHL1* emerged as one of the top candidate genes (Table S3). Compared with non-responders, clinical data from the R2 Platform revealed significantly lower UCHL1 expression levels in patients who responded to anti-HER2 therapy, either as monotherapy or combined with chemotherapy (Fig. 1B). Baseline clinicopathological features are summarized in Table S4. Furthermore, high UCHL1 levels were correlated with the resistance of HER2-targeted agents, such as afatinib in the GSCA database (Fig. S1A). Kaplan-Meier analysis of the HER2-positive breast cancer cohort revealed that UCHL1 overexpression was associated with poorer overall survival (OS), relapse-free survival (RFS), post-progression survival (PPS), and distant metastasis-free survival (DMFS) (Fig. 1C). Collectively, these findings identify UCHL1 as a candidate molecule that may drive poor prognosis and therapeutic resistance in HER2-positive breast cancer.

To investigate the role of UCHL1 in resistance to anti-HER2-targeted therapy, represented by pyrotinib, in HER2-positive breast cancer, we first classified breast cancer cell lines into HER2-negative (SUM159 and MDA-MB-231) and HER2-positive (BT474 and SK-BR-3) groups based on HER2 expression (Fig. S1B).

Both mRNA and protein levels of UCHL1 were markedly elevated in HER2-positive cells compared with HER2-negative cells (Fig. S1C-D). Compared with HER2-negative cells, HER2-positive cells were significantly more sensitive to pyrotinib, as determined by CCK-8 assays (Fig. S1E). We successfully established pyrotinib-resistant SK-BR-3-R cells with stable pyrotinib resistance and altered morphology, and western blotting, qPCR and immunofluorescence analyses verified that UCHL1 was upregulated in SK-BR-3-R cells compared with parental cells (Fig. 1D-G). CCK-8 assays indicated that the IC_{50} of pyrotinib in SK-BR-3-R cells was approximately 140-fold higher than that in parental SK-BR-3 cells (4 150 nM vs. 29.51 nM), and colony formation assays consistently revealed that SK-BR-3-R cells retained robust clonogenic capacity upon pyrotinib treatment (Fig. S1F-G). These results suggest that higher UCHL1 expression is correlated with pyrotinib resistance in HER2-positive breast cancer.

UCHL1 conferred pyrotinib resistance in HER2-positive breast cancer

We used shRNA to knock down UCHL1 expression in SK-BR-3-R cells. Among the three constructs, sh*UCHL1*-3 exhibited the highest knockdown efficiency (Fig. 2A-B) and was thus selected for all subsequent experiments, with immunofluorescence staining further confirming efficient knockdown of *UCHL1* in SK-BR-3-R-sh*UCHL1* cells (Fig. 2C). CCK-8 assays revealed a decrease in IC_{50} from 4 763 nM in SK-BR-3-R-shNC cells to 103.8 nM in -sh*UCHL1* cells (Fig. 2D), and colony formation assays consistently showed that SK-BR-3-R-sh*UCHL1* cells displayed increased pyrotinib sensitivity relative to -shNC cells (Fig. 2E). Concurrently, UCHL1 overexpression in parental SK-BR-3 cells increased the IC_{50} of pyrotinib from 261.2 nM to 1 668 nM and enhanced colony-forming capacity under pyrotinib treatment (Fig. 2F-H), and the same findings were also observed in BT474 cells (Fig. S2A-C). These results validate UCHL1 as a critical driver gene of pyrotinib resistance in HER2-positive breast cancer.

UCHL1 promoted pyrotinib resistance by enhancing autophagy and DDR in HER2-positive breast cancer

To dissect the molecular mechanisms underlying UCHL1-mediated pyrotinib resistance, RNA-seq transcriptomic profiling was performed, and pathway enrichment analysis revealed that phagolysosome assembly and phagosome-lysosome fusion pathways were associated with UCHL1 (Fig. 3A). Autophagic flux was impaired in pyrotinib-treated SK-BR-3-R-sh*UCHL1* cells (Fig. 3B), and western blotting showed reduced Beclin 1 and LC3-Ⅱ levels alongside p62 accumulation in these cells (Fig. 3C). Treatment of SK-BR-3-R cells with the autophagy inhibitor chloroquine (CQ) markedly reduced the IC_{50} of pyrotinib, from 3 847 nM to 136.2 nM (Fig. S3), supporting UCHL1-dependent autophagy in pyrotinib resistance. It was verified that UCHL1 contributes to autophagy activation in HER2-positive breast cancer.

USP-family deubiquitinases were also reported to regulate DDR, and ROS-induced DNA damage mediates TKI resistance in tumors [28]. Accumulating evidence reveals the crosstalk exists between DDR and autophagy [29]. Immunofluorescence assay indicated that pyrotinib-triggered DNA damage was

exacerbated in SK-BR-3-R-sh*UCHL1* cells, accompanied by increased γ-H2AX (Fig. 3D). Furthermore, *UCHL1* knockdown impaired the induction of DNA repair proteins TOP2A and MSH2 following treatment with pyrotinib (Fig. 3E), suggesting impaired DNA repair capacity. Moreover, intracellular ROS levels further increased upon *UCHL1* knockdown (Fig. 3F), and comet assays revealed that *UCHL1* knockdown markedly amplified pyrotinib-induced DNA fragmentation (Fig. 3G). Collectively, these data indicate that UCHL1 drives pyrotinib resistance by promoting autophagy and DDR in HER2-positive breast cancer.

UCHL1 mediated pyrotinib resistance by deubiquitinating SLC25A5 in HER2-positive breast cancer

We futher elucidated the mechanism underlying UCHL1-driven resistance to pyrotinib. Cross-referencing UCHL1-interacting proteins from IP-MS and *UCHL1*-correlated genes in HER2-positive breast cancer cohorts identified SLC25A5 as a high-confidence candidate (Fig. 4A). Co-immunoprecipitation assays confirmed the interaction between UCHL1 and SLC25A5 (Fig. 4B). Our findings indicated that SLC25A5 protein stability was compromised in the absence of UCHL1 (Fig. 4C). Additionally, the proteasome inhibitor MG132 reversed the reduction in SLC25A5 levels caused by UCHL1 knockdown, suggesting that SLC25A5 degradation was mediated by the proteasome pathway (Fig. 4D). Collectively, these findings suggest that UCHL1 stabilizes SLC25A5 protein and prevents its degradation via the ubiquitin-proteasome pathway.

We generated a catalytically inactive UCHL1 mutant (C90S) [30] to assess the role of its deubiquitinase activity. Overexpression of the wild-type UCHL1, but not C90S, suppressed the ubiquitination of SLC25A5 (Fig. 4E). Using linkage-specific ubiquitin constructs, we found that UCHL1 selectively catalyzes K11 (lysine 11)-linked deubiquitination of SLC25A5, which was abrogated by the K11R (lysine 11-to-arginine) mutant ubiquitin (Fig. 4F-G). Co-IP assays demonstrated that the M1 region (residues 1-151) is essential for the UCHL1- SLC25A5 interaction (Fig. 4H). Collectively, UCHL1 maintained SLC25A5 stability by removing K11-linked ubiquitin chains.

Functionally, SLC25A5 overexpression partly reversed the impaired proliferation of SK-BR-3-R cells upon *UCHL1* knockdown (Fig. S4A-B), and restoring SLC25A5 consistently rescued protective autophagy while attenuating DDR signaling triggered by *UCHL1* knockdown (Fig. S4C-D). Collectively, UCHL1-mediated deubiquitination of SLC25A5 preserved its stability and promoted autophagy and DDR, thereby conferring pyrotinib resistance.

The UCHL1 inhibitor enhanced the sensitivity of HER2-positive breast cancer cells to pyrotinib and DOX

The UCHL1 inhibitor LDN significantly sensitized SK-BR-3-R cells to pyrotinib, lowering the IC_{50} from 4 360 nM to 139.1 nM (Fig. 5A). Consistently, the colony formation assay confirmed that co-treatment with LDN and pyrotinib more effectively suppressed clonogenic growth compared to pyrotinib (Fig. 5B). IHC staining of HER2-positive breast cancer specimens revealed elevated expression of UCHL1 and SLC25A5 in pyrotinib-resistant tumors compared to sensitive cases (Fig. 5C). Consistently, SK-BR-3-R

cells treated with LDN significantly reduced the IC_{50} of anthracycline agent DOX, from 1 980 nM (DMSO) to 235.7 nM (Fig. 5D). These findings suggest that UCHL1 inhibition may enhance the therapeutic efficacy of both the HER-TKI pyrotinib and the anthracycline DOX.

We further verified the function of UCHL1 on HER2-positive breast cancer *in vivo*. No obvious body-weight loss was observed among the groups in this orthotopic model (Fig. 5E). The TUBO-*UCHL1* group exhibited enhanced tumor growth under pyrotinib monotherapy compared with the vector group (Fig. S5A-C). The combination of LDN with pyrotinib produced superior antitumor efficacy compared with single-agent treatment in the TUBO-*UCHL1* group (Fig. 5F-H). IHC staining showed that LDN treatment altered SLC25A5 protein abundance (Fig. 5I). Collectively, these data suggest that pharmacological inhibition of UCHL1 restored tumor sensitivity to pyrotinib in HER2-positive breast cancer.

The prognostic significance of UCHL1-SLC25A5 axis in HER2-positive breast cancer

Kaplan-Meier survival analysis revealed that SLC25A5 overexpression correlates with worse OS, RFS, and DMFS in HER2-positive breast cancer (Fig. S6A), and multivariate analysis further correlated high SLC25A5 expression with malignant progression of breast cancer (Fig. S6B). Compared with normal mammary tissue, SLC25A5 was markedly up-regulated across breast cancer subtypes, with the highest median expression observed in HER2-positive subtype (Fig. 6A).

To further evaluate the clinical prognostic value of the UCHL1-SLC25A5 axis, TCGA analysis was performed and showed that concurrent overexpression of UCHL1 and SLC25A5 was associated with poorer prognosis in HER2-positive breast cancer, compared with the low-coexpression group (Fig. 6B). Overall, the UCHL1-SLC25A5 axis facilitates resistance to pyrotinib in HER2-positive breast cancer (Fig. 6C).

DISCUSSION

This study provides both clinical and experimental evidences supporting the critical role of UCHL1 in driving pyrotinib resistance in HER2-positive breast cancer. We found that high expression of UCHL1 was closely associated with pyrotinib resistance and poor clinical prognosis in HER2-positive breast cancer, based on IHC assessment of clinical tumor specimens. Overexpressed UCHL1 induced pyrotinib resistance in sensitive cells, while genetic intervention of UCHL1 reversed its resistance. Mechanistically, UCHL1 overexpression was shown to increase LC3-□ levels, reduce γ-H2AX, and limit ROS accumulation upon pyrotinib treatment. UCHL1 deubiquitinated and stabilized SLC25A5, thereby activating autophagy and enhancing DDR. Collectively, these mechanisms regulated by UCHL1 promoted cell survival and conferred pyrotinib resistance in HER2-positive breast cancer.

In breast cancer, UCHL1 drives endocrine therapy resistance by stabilizing KLF5 [31]. Our findings also revealed that elevated UCHL1 expression contributed to doxorubicin resistance in HER2-breast cancer [19]. Notably, UCHL1 has been reported to suppress HER2 expression and enhance sensitivity to the

HER2-TKI lapatinib [32]. Nevertheless, whether UCHL1 regulates pyrotinib resistance in HER2-positive breast cancer has not been clarified. Bioinformatic analyses in our study reveal that UCHL1 expression is significantly correlated with TKI resistance and unfavorable clinical prognosis in HER2-positive breast cancer. Inhibition of UCHL1 not only regulates cellular sensitivity to pyrotinib but also affects the chemotherapeutic response to doxorubicin. Collectively, these findings suggest that UCHL1 may serve as an effective therapeutic target for HER2-positive breast cancer and provide a theoretical basis for optimizing regimens combining TKI therapy with anthracycline-based chemotherapy.

Most previous studies have investigated autophagy or DDR separately in HER2-TKI resistance. Chen *et al.* demonstrated that prolonged lapatinib treatment induces protective autophagy in HER2-positive breast cancer cells [33]. On the other hand, lapatinib directly disrupts the DNA-binding activity of the NER factor DDB2, thereby enhancing chemotherapy sensitivity in HER2-positive breast cancer [9]. However, the function of UCHL1 on autophagy and DDR in mediating pyrotinib resistance remain unclear. Here, our data demonstrate that UCHL1 governs both protective autophagy and enhanced DDR to remodel the resistance to HER2-TKI pyrotinib. Moreover, we identify SLC25A5 as a novel functional target of UCHL1, whereby UCHL1-mediated K11-linked deubiquitination and stabilization of SLC25A5 simultaneously enhances autophagy and DDR signaling, driving adaptive pyrotinib resistance. Altogether, UCHL1 acts as a key regulator of HER2-targeted therapy, representing a promising interventional target in HER2-positive breast cancer.

Currently, dual blockade with trastuzumab plus pertuzumab is the standard first-line regimen in HER2-positive breast cancer [34]. In China, pyrotinib combined with chemotherapy exhibits superior efficacy compared with lapatinib-based regimens [35]. Nevertheless, pyrotinib resistance remains a clinical challenge [36], and effective strategies to overcome resistance are still lacking. Notably, our data showed that specific the small-molecule inhibitor of UCHL1 (LDN) could efficiently reverse the resistance of HER2-positive breast cancer cells to both anti-HER2 agent pyrotinib and DOX, further substantiating the central regulatory function of UCHL1 in therapeutic resistance. Co-overexpression of UCHL1 and SLC25A5 predicts advanced disease stage and poor prognosis in HER2-positive breast cancer, with survival analyses validating the prognostic performance of the UCHL1-SLC25A5 axis. Taken together, pharmacological intervention targeting UCHL1 serves as an effective therapeutic strategy against HER2-targeted resistance in tumor.

Our study unraveled the role of UCHL1-SLC25A5 axis in pyrotinib resistance in HER2-positive breast cancer. However, this study still has several limitations. The sample size was relatively small, and multi-center cohort validation is needed to confirm the prognostic value of UCHL1. Moreover, the molecular mechanisms through which UCHL1 deubiquitinates SLC25A5 also warrant further in-depth studies. Finally, the role of UCHL1 in modulating resistance to other DNA-damaging agents, such as platinum compounds and PARP inhibitors, remains to be explored.

In conclusion, the UCHL1-SLC25A5 axis drives pyrotinib and DOX resistance by orchestrating autophagy and DDR in HER2-positive breast cancer. Our findings suggest UCHL1 as an effective prognostic

biomarker and therapeutic target for clinical treatment of HER2-positive breast cancer.

Declarations

ETHICS APPROVAL AND CONSENT TO PARTICIPATE

All participants provided written informed consent. The study protocol was reviewed and approved by the Ethics Committee of Suzhou Municipal Hospital (approval number: K-2024-147-K01), in compliance with the guidelines stipulated in the Declaration of Helsinki.

CONSENT FOR PUBLICATION

All authors have approved the manuscript and agreed to its publication.

COMPETING INTERESTS

The authors declare that they have no competing interests.

FUNDING INFORMATION

This study was supported by grants from the National Natural Science Foundation of

China (Grant No. 82272871), Suzhou Municipal Young Science and Technology Talent Support Program (Grant No. 2025 – 159), Suzhou Basic Science and Technology Project (Grant No. SYWD2024263), China Foundation for International Medical Exchange (Grant No. Z-2021-46-2101-2023), Suzhou Youth Science and Technology Project (Grant No. KJXW2023034), Jiangsu Hengrui Pharmaceutical Clinical Pharmacy Research Fund (Grant No. H202114), Changzhou Siyao Pharmaceutical Clinical Pharmacy Research Fund (Grant No. SKYXD2022028), Suzhou Science and Technology Development Plan Project (Grant No. SKY2022198), Jiangsu Pharmaceutical Association Research Project (Grant No. Q202233), Nanjing Medical University-Qilu Clinical Research Fund (Grant No. 2024KF0265), Jiangsu Association of Research Hospitals Precision Medication Fund (Grant No. JY202202), Natural Science Foundation of Gusu School of Nanjing Medical University (Grant No. GSKY202610306, GSKY20260904, szslyypmd2026002) and the Natural Science Foundation of Jiangsu Higher Education Institutions (Grant No. 21KJB320017).

AUTHOR CONTRIBUTIONS

YY and XD were responsible for conceptualization. YZ, QL, JW, JX, ZW, RH, MX and GX performed the experiments and analyzed the data. YY managed data curation. JX and YZ wrote the manuscript, and XYD revised the manuscript. All the authors read and approved the manuscript for publication.

ACKNOWLEDGMENTS

The authors thank the public databases, including K-M Plot, GSCA, R2 Platform, for providing their platforms and the contributors for uploading their valuable datasets. We also acknowledge BioRender for providing the illustration tools used to create the figures in this manuscript. This study was supported by the Laboratory Animal Center of Suzhou Vocational Health College, which provided technical support and platform resources.

DATA AVAILABILITY STATEMENT

All web links are described in the “Methods” section. Datasets used and/or analyzed during the current study are available from the corresponding author on reasonable request.

References

1. Torres JM, Sodipo MO, Hopkins MF, Chandler PD, Warner ET. Racial differences in breast cancer survival between black and white women according to tumor subtype: a systematic review and meta-analysis. J Clin Oncol 2024, 42(32): 3867–3879.
2. Yoon J, Oh DY. HER2-targeted therapies beyond breast cancer - an update. Nat Rev Clin Oncol 2024, 21(9): 675–700.
3. Zheng Y, Cao WM, Shao X, Shi Y, Cai L, Chen W, et al. Pyrotinib plus docetaxel as first-line treatment for HER2-positive metastatic breast cancer: the PANDORA phase II trial. Nat Commun 2023, 14(1): 8314.
4. Angelis V, Okines AFC. Systemic therapies for HER2-positive advanced breast cancer. Cancers (Basel) 2023, 16(1): 15.
5. Chen H, Si Y, Wen J, Hu C, Xia E, Wang Y, et al. P110α inhibitor alpelisib exhibits a synergistic effect with pyrotinib and reverses pyrotinib resistant in HER2 + breast cancer. Neoplasia 2023, 43: 100913.
6. Wang E, Mi X, Thompson MC, Montoya S, Notti RQ, Afaghani J, et al. Mechanisms of resistance to noncovalent bruton's tyrosine kinase inhibitors. N Engl J Med 2022, 386(8): 735–743.
7. Liu X, Zhang X, Shao Z, Zhong X, Ding X, Wu L, et al. Pyrotinib and chrysin synergistically potentiate autophagy in HER2-positive breast cancer. Signal transduction and targeted therapy 2023, 8(1): 463.
8. Wang Y, Zhou Q, Liu C, Zhang R, Xing B, Du J, et al. Targeting IL-6/STAT3 signaling abrogates EGFR-TKI resistance through inhibiting Beclin-1 dependent autophagy in HNSCC. Cancer Lett 2024, 586: 216612.
9. Hsu SC, He YH, Chen YJ, Le UNP, Liu PT, Huynh TK, et al. Disrupting DDB2-DNA interaction by lapatinib enhances chemotherapy sensitivity. International journal of biological sciences 2025, 21(14): 6007–6024.

10. Lee J, Kida K, Koh J, Liu H, Manyam GC, Gi YJ, et al. The DNA repair pathway as a therapeutic target to synergize with trastuzumab deruxtecan in HER2-targeted antibody-drug conjugate-resistant HER2-overexpressing breast cancer. Journal of experimental & clinical cancer research: CR 2024, 43(1): 236.
11. Garcia-Mayea Y, Mir C, Masson F, Paciucci R, ME LL. Insights into new mechanisms and models of cancer stem cell multidrug resistance. Seminars in cancer biology 2020, 60: 166–180.
12. Han D, Wang L, Jiang S, Yang Q. The ubiquitin-proteasome system in breast cancer. Trends Mol Med 2023, 29(8): 599–621.
13. Xia L, Xing Y, Ye X, Wu Y, Yang Y, Yin Z, et al. TRIM21-driven K63-linked ubiquitination of RBM38c, as a novel interactor of BECN1, contributes to DNA damage-induced autophagy. Cell Death Differ 2025, 32(6): 1158–1175.
14. Li Y, Li L, Wang X, Zhao F, Yang Y, Zhou Y, et al. USP25 elevates SHLD2-mediated DNA double-strand break repair and regulates chemoresponse in cancer. Adv Sci (Weinh) 2024, 11(28): e2403485.
15. Bao L, Wang X, Liao X, Li D, Li C, Dai N, et al. Pyrotinib targeted EGFR/GRP78 mediated cell apoptosis in high EGFR gene copy number gastric cancer. Journal of experimental & clinical cancer research: CR 2025, 44(1): 245.
16. Li X, Wang J, Li S, Fang J, Hao Y, Xu C, et al. Pyrotinib inhibits the tumorigenicity of HER2-positive non-small cell lung cancer by inducing ARIH1/ubiquitin/lysosome-dependent degradation of HER2. Cellular oncology (Dordrecht, Netherlands) 2025, 48(6): 1795–1808.
17. Kwan SY, Au-Yeung CL, Yeung TL, Rynne-Vidal A, Wong KK, Risinger JI, et al. Ubiquitin carboxyl-terminal hydrolase L1 (UCHL1) promotes uterine serous cancer cell proliferation and cell cycle progression. Cancers (Basel) 2020, 12(1): 118.
18. Lu G, Li J, Ding L, Wang C, Tang L, Liu X, et al. The deubiquitinating enzyme UCHL1 induces resistance to doxorubicin in HER2 + breast cancer by promoting free fatty acid synthesis. Front Oncol 2021, 11: 629640.
19. Ding X, Gu Y, Jin M, Guo X, Xue S, Tan C, et al. The deubiquitinating enzyme UCHL1 promotes resistance to pemetrexed in non-small cell lung cancer by upregulating thymidylate synthase. Theranostics 2020, 10(13): 6048–6060.
20. Zheng R, Chen X, Xu G, Liu Q, Hu S, Shi H, et al. UCHL1 promotes temozolomide resistance in glioblastoma by inhibiting the ubiquitination-mediated degradation of keratin 8. Translational oncology 2026, 67: 102728.
21. Collins A, Møller P, Gajski G, Vodenková S, Abdulwahed A, Anderson D, et al. Measuring DNA modifications with the comet assay: a compendium of protocols. Nature protocols 2023, 18(3): 929–989.
22. Ren Y, Zhou F, Tan Z, Yang S, Zhang S, Zhang Y, et al. OTUD4 deubiquitination stabilizes EGFR and activates the PI3K/AKT pathway to promote the invasiveness of triple-negative breast cancer. Cell Death Dis 2026, 17(1):245.

23. Liu S, Lan B, Wang Y, Yang T, Li L, Ge H, et al. Pyrotinib and trastuzumab combination treatment synergistically overcomes HER2 dependency in HER2-positive breast cancer: insights from the PHILA trial. EBioMedicine 2024, 109: 105379.
24. Gong B, Cao Z, Zheng P, Vitolo OV, Liu S, Staniszewski A, et al. Ubiquitin hydrolase Uch-L1 rescues beta-amyloid-induced decreases in synaptic function and contextual memory. Cell 2006, 126(4): 775–788.
25. Narayanan S, Cai CY, Assaraf YG, Guo HQ, Cui Q, Wei L, et al. Targeting the ubiquitin-proteasome pathway to overcome anti-cancer drug resistance. Drug Resist Updat 2020, 48: 100663.
26. Liu CJ, Hu FF, Xie GY, Miao YR, Li XW, Zeng Y, et al. GSCA: an integrated platform for gene set cancer analysis at genomic, pharmacogenomic and immunogenomic levels. Brief Bioinform 2023, 24(1):bbac558.
27. Győrffy B. Integrated analysis of public datasets for the discovery and validation of survival-associated genes in solid tumors. Innovation (Camb) 2024, 5(3): 100625.
28. Zhang H, Yan H, Liu Y, Zeng A, Song L. The ubiquitination-autophagy axis in cancer therapy resistance: mechanistic insights and therapeutic opportunities. Front Pharmacol 2025, 16: 1722559.
29. Singh A, Ravendranathan N, Frisbee JC, Singh KK. Complex interplay between DNA damage and aAutophagy in disease and therapy. Biomolecules 2024, 14(8):922.
30. Mondal M, Conole D, Nautiyal J, Tate EW. UCHL1 as a novel target in breast cancer: emerging insights from cell and chemical biology. Br J Cancer 2022, 126(1): 24–33.
31. Li J, Liang Y, Zhou S, Chen J, Wu C. UCHL1 contributes to insensitivity to endocrine therapy in triple-negative breast cancer by deubiquitinating and stabilizing KLF5. Breast Cancer Res 2024, 26(1): 44.
32. Zheng M, Chen X, Gan W, Hou L, Zhou Z, Chen C, et al. UCH-L1 down-regulates HER2 expression and increases lapatinib sensitivity by interacting with HSP90 in HER2-positive breast cancer. Genes & diseases 2026, 13(4): 101952.
33. Chen S, Zhu X, Qiao H, Ye M, Lai X, Yu S, et al. Protective autophagy promotes the resistance of HER2-positive breast cancer cells to lapatinib. Tumour biology: the journal of the International Society for Oncodevelopmental Biology and Medicine 2016, 37(2): 2321–2331.
34. Swain SM, Shastry M, Hamilton E. Targeting HER2-positive breast cancer: advances and future directions. Nature reviews Drug discovery 2023, 22(2): 101–126.
35. Xu B, Yan M, Ma F, Hu X, Feng J, Ouyang Q, et al. Pyrotinib plus capecitabine versus lapatinib plus capecitabine for the treatment of HER2-positive metastatic breast cancer (PHOEBE): a multicentre, open-label, randomised, controlled, phase 3 trial. The Lancet Oncology 2021, 22(3): 351–360.
36. Harbeck N, Penault-Llorca F, Cortes J, Gnant M, Houssami N, Poortmans P, et al. Breast cancer. Nature reviews Disease primers 2019, 5(1): 66.

Figures

Figure 1

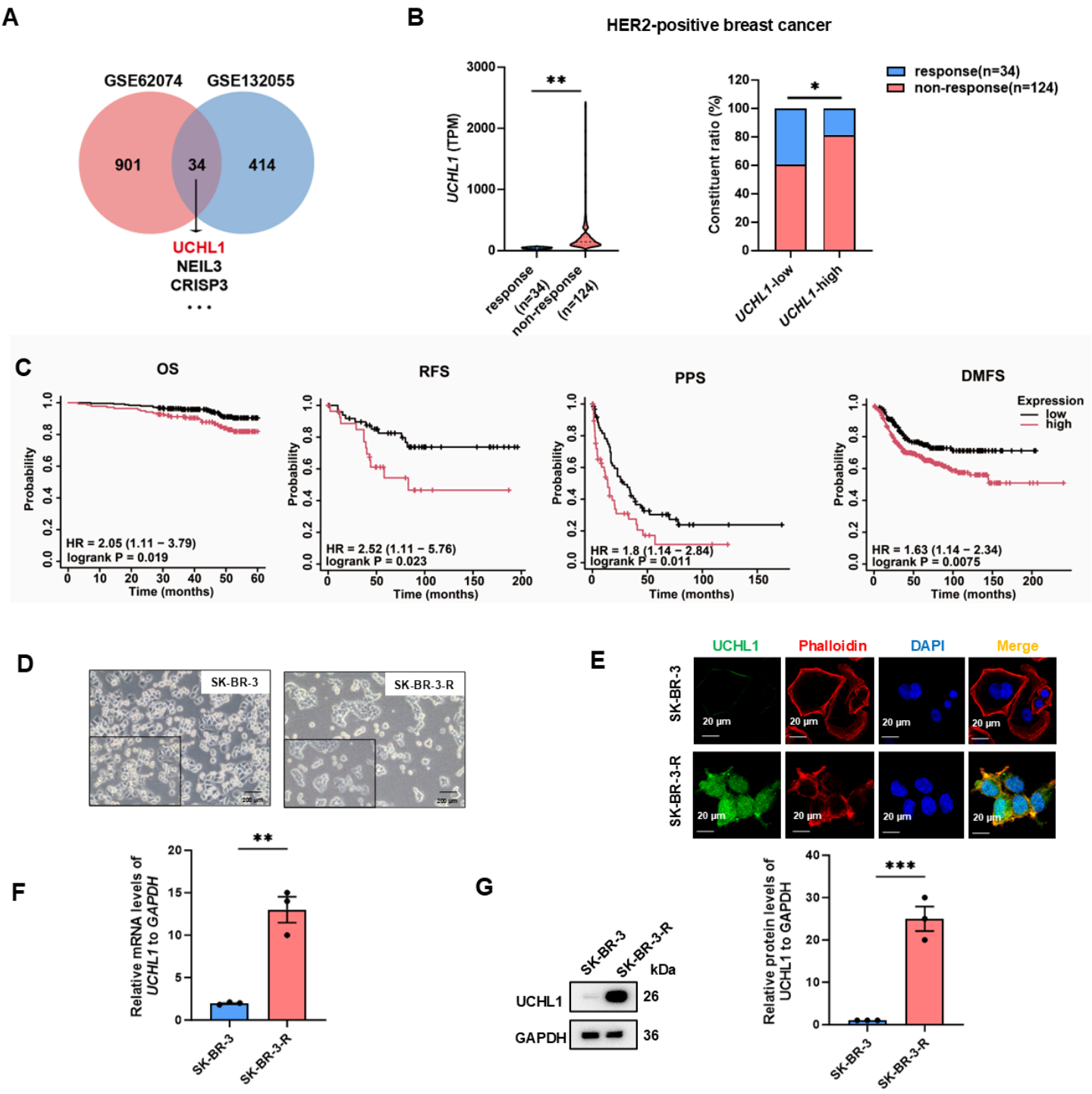


Figure 1

Association of UCHL1 expression with pyrotinib resistance in HER2-positive breast cancer. A Differentially expressed genes derived from GEO datasets GSE132055 and GSE62074 were intersected with a panel of ubiquitin-related proteases to screen candidate genes. **B** UCHL1 expression levels were compared between pyrotinib responders (n=34) and non-responders (n=124) with HER2-positive breast cancer via the R2 Genomics Platform. **C** Kaplan-Meier survival analyses were performed to evaluate the

correlation between UCHL1 expression and OS, RFS, PPS and DMFS in patients with HER2-positive breast cancer. **D** Representative images of cells from the parental cell line SK-BR-3 and the drug-resistant cell line SK-BR-3-R (scale bars, 200 μm). **E** Immunofluorescence staining was performed to visualize UCHL1 expression in SK-BR-3 and SK-BR-3-R cell lines (scale bars, 20 μm). **F-G** WB and qPCR were used to detect UCHL1 protein and *UCHL1* mRNA expression across the indicated cell lines, respectively (n=3). Error bars represent Mean ± SEM. $^{*}P < 0.05$, $^{**}P < 0.01$, $^{***}P < 0.001$.

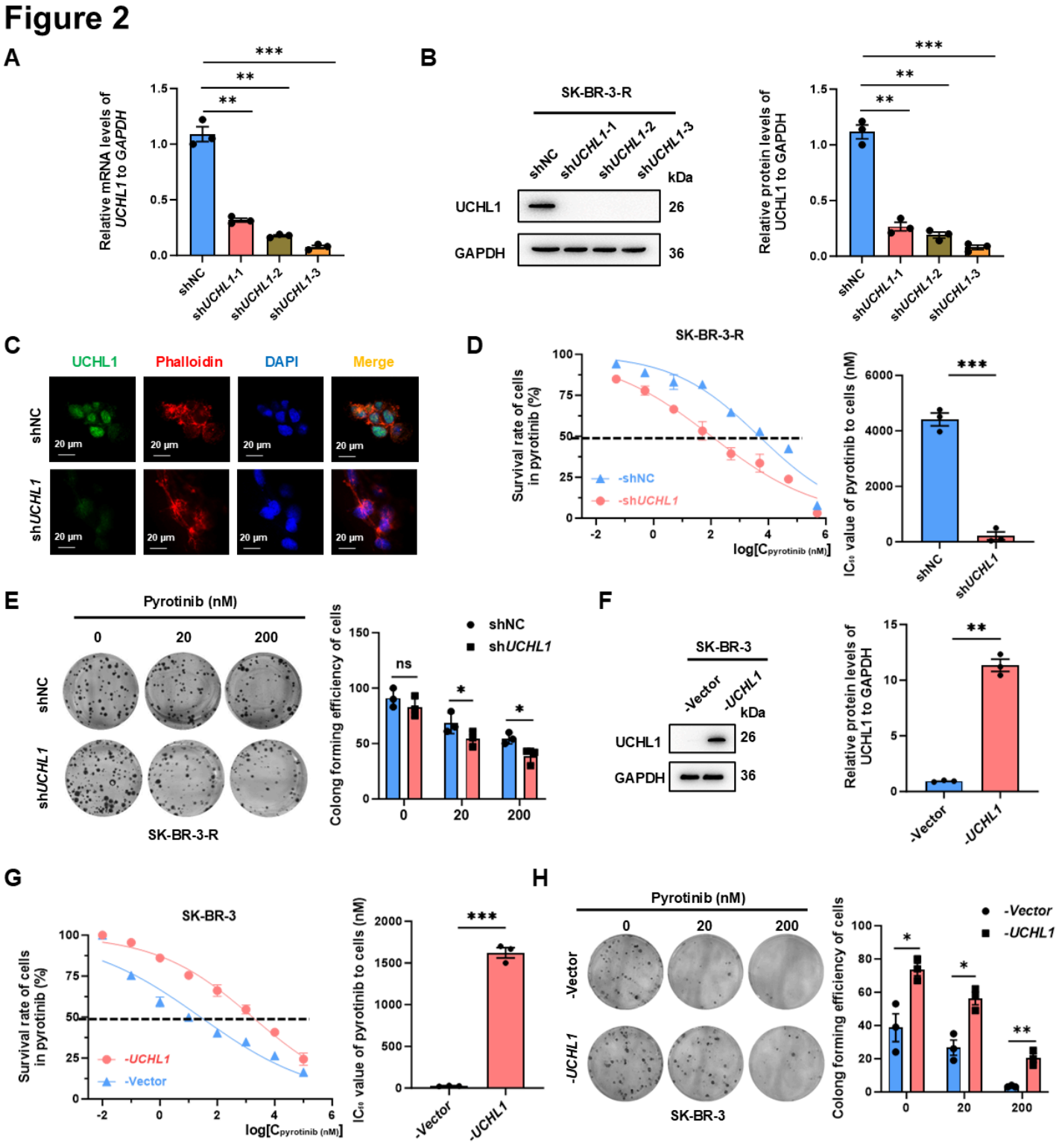


Figure 2

UCHL1 confers pyrotinib resistance in HER2-positive breast cancer. A-B WB and qPCR were performed to detect UCHL1 protein and *UCHL1* mRNA expression across the indicated cell lines, respectively (n=3). Error bars represent Mean ± SEM. **C** Immunofluorescence staining was performed to detect UCHL1 expression in the indicated cell groups (scale bars, 20 μm). **D** Cell viability was evaluated via the CCK-8 assay in the indicated cell groups (n=3). Error bars represent Mean ± SEM. **E** Colony formation assays were employed to assess pyrotinib sensitivity in the indicated cell groups (n=3). Error bars represent Mean ± SEM. **F** WB was performed to detect UCHL1 protein expression in the indicated cell groups (n=3). Error bars represent Mean ± SEM. **G** Cell viability was measured using the CCK-8 assay in the indicated cell groups (n=3). Error bars represent Mean ± SEM. **H** Colony formation assays were utilized to evaluate pyrotinib sensitivity in the indicated cell groups (n=3). Error bars represent Mean ± SEM. $^{*}P < 0.05$, $^{**}P < 0.01$, $^{***}P < 0.001$.

Figure 3

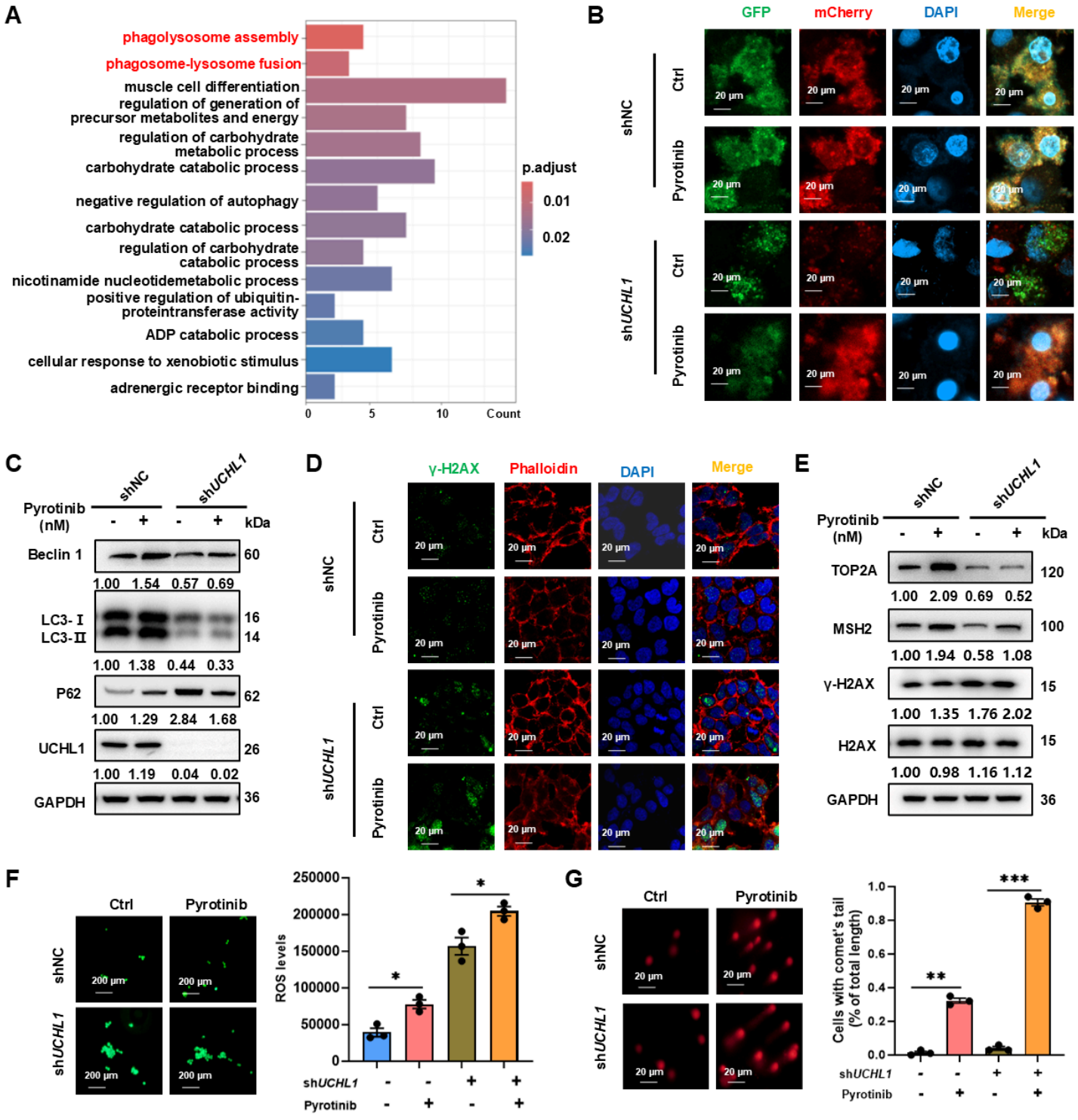


Figure 3

UCHL1 promotes pyrotinib resistance by enhancing autophagy and DDR in HER2-positive breast cancer. A GO enrichment analysis displaying the top functional terms of RNA-seq-derived differentially expressed genes. Bar length represents gene count, and color indicates adjusted *P*-value. **B** SK-BR-3-R-shNC and -sh*UCHL1* cells were transfected with mCherry-GFP-LC3 plasmid (Cat# PPL00191-2d, Public Protein/Plasmid Library, Nanjing, China), followed by treatment with pyrotinib. Representative confocal

images show autophagosomes (yellow puncta) and autolysosomes (red puncta) (scale bars, 20 μm). **C** WB was conducted to assess the expression of UCHL1 and autophagy-associated proteins (Beclin 1, LC3, p62) across the indicated groups. **D** Immunofluorescence staining was performed to detect γ-H2AX expression in the indicated groups (scale bars, 20 μm). **E** WB was performed to analyze the levels of DNA damage marker γ-H2AX and DNA repair-related proteins (TOP2A, MSH2) in the indicated groups. **F** Intracellular ROS abundance in each group was measured using the ROS Fluorometric Assay Kit (Green, n=3, scale bars, 200 μm). Error bars represent Mean ± SEM. **G** Comet assays were carried out to quantify DNA damage in the indicated groups (n=3, scale bars, 20 μm). Error bars represent Mean ± SEM. $^{*}P < 0.05$, $^{**}P < 0.01$, $^{***}P < 0.001$.

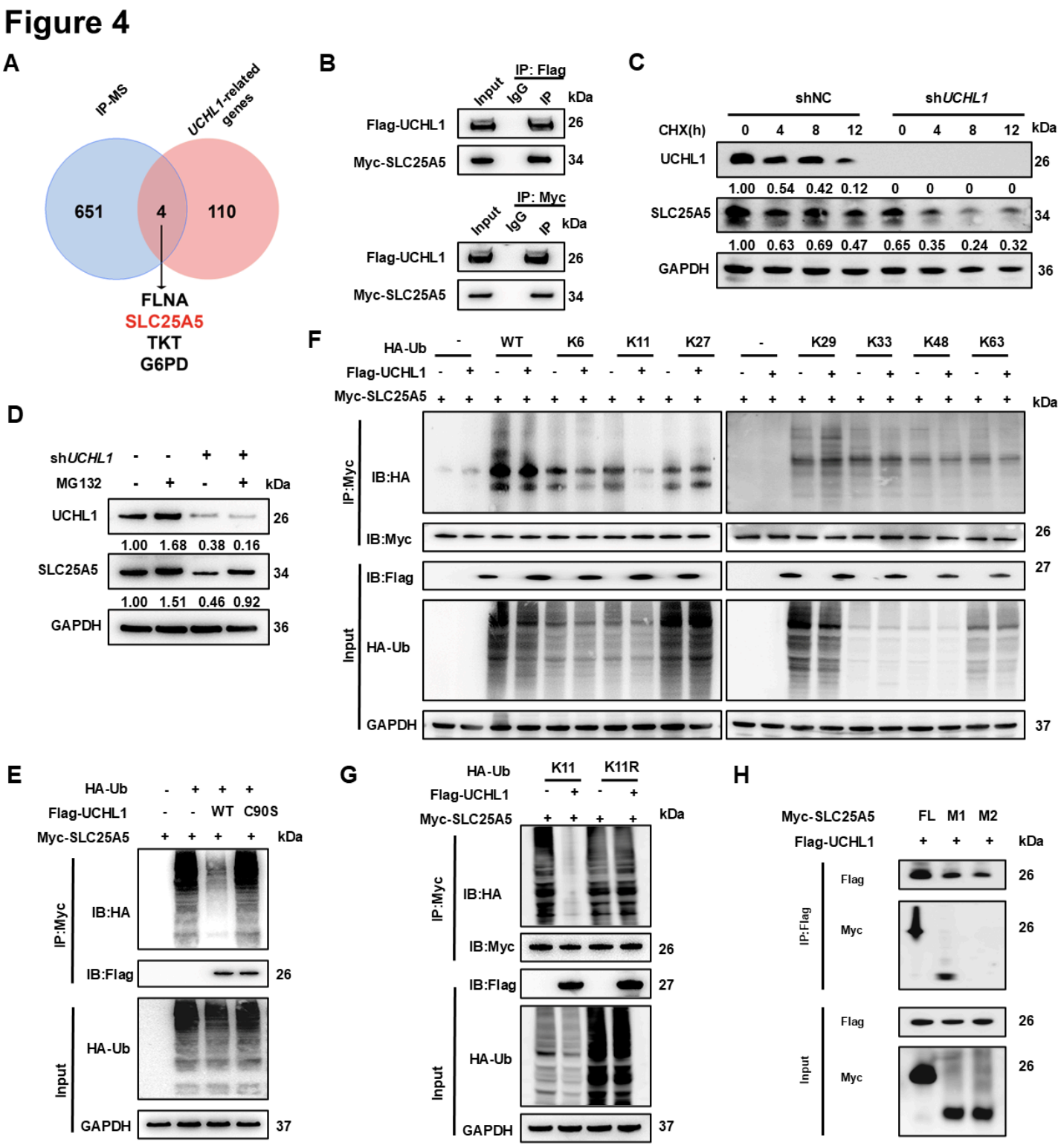


Figure 4

UCHL1 mediates pyrotinib resistance by deubiquitinating SLC25A5 in HER2-positive breast cancer. A Endogenous UCHL1 was immunoprecipitated from SK-BR-3-R cells, and interacting proteins were overlapped with a panel of *UCHL1*-associated genes. **B** Co-IP assays were performed to verify the physical interaction between UCHL1 and SLC25A5. **C** WB was used to detect SLC25A5 protein half-life following treatment with cycloheximide (CHX, 20 μg/mL). **D** WB was used to detect protein abundance in

each group after MG132 (20 μM) treatment. **E** Ubiquitination assays using HA-ubiquitin and the UCHL1 catalytic mutant (C90S) revealed that UCHL1 enzymatic activity is required for SLC25A5 deubiquitination. **F**Ubiquitination assays were conducted in 293T cells co-transfected with Flag-UCHL1, Myc-SLC25A5, and linkage-specific ubiquitin plasmids (K6, K11, K27, K29, K33, K48, K63). **G** Ubiquitination assays were performed using cells co-transfected with Flag-UCHL1, Myc-SLC25A5, and K11 linkage-specific ubiquitin constructs (K11, K11R). **H** Co-IP assays in 293T cells were conducted to detect binding between UCHL1 and SLC25A5 deletion mutants (1-151, 152-298).

Figure 5

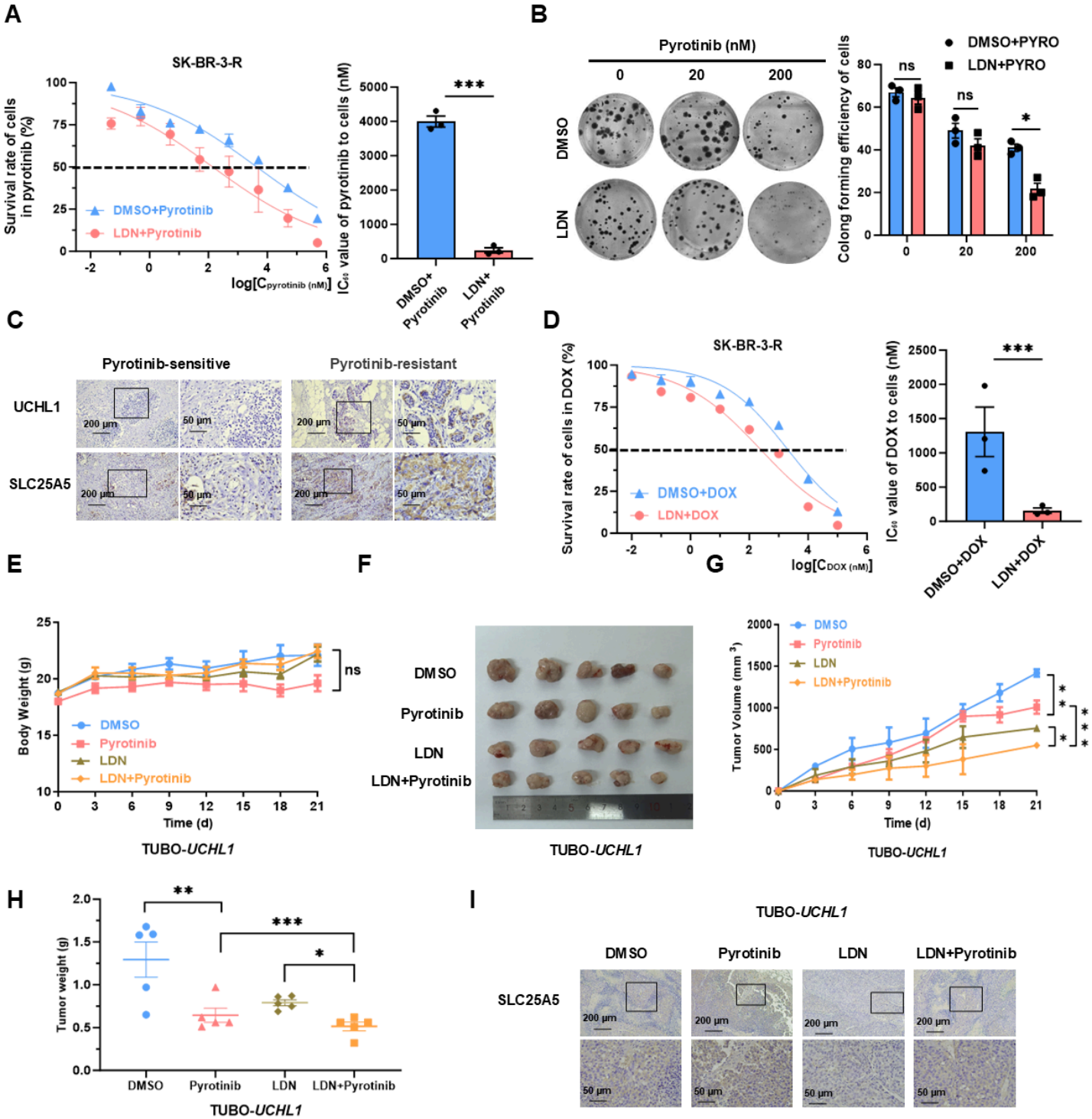


Figure 5

The UCHL1 inhibitor enhances the sensitivity of HER2-positive breast cancer cells to pyrotinib and DOX. A Cell viability was assessed via the CCK-8 assay across the indicated groups (n=3). Error bars represent Mean ± SEM. **B** Colony formation assays were used to detect cell viability of SK-BR-3-R under distinct treatment regimens (n=3). Error bars represent Mean ± SEM. **C** Immunohistochemical staining was performed to detect UCHL1 and SLC25A5 expression in pyrotinib-sensitive and resistant tumor tissues (scale bars: 200 μm (main panel); inset, 50 μm). **D** The CCK-8 assay was applied to evaluate cell viability of SK-BR-3-R in different treatment groups (n=3). Error bars represent Mean ± SEM. **E-H** Orthotopic breast cancer models were constructed to explore the regulatory role of the UCHL1 axis in tumor progression. Mice received pyrotinib (10 mg/kg) via intragastric administration every three days (n=5 per group). Error bars represent Mean ± SEM. **E** Animal body weight curves. **F** Representative tumor photographs. **G** Tumor volume statistics. **H** Tumor weight measurements. **I** IHC analysis was conducted to detect SLC25A5 expression in mouse tumor tissues (scale bars: 200 μm (main panel); inset, 50 μm). ns, not significant. $^{*}P < 0.05$, $^{**}P < 0.01$, $^{***}P < 0.001$.

Figure 6

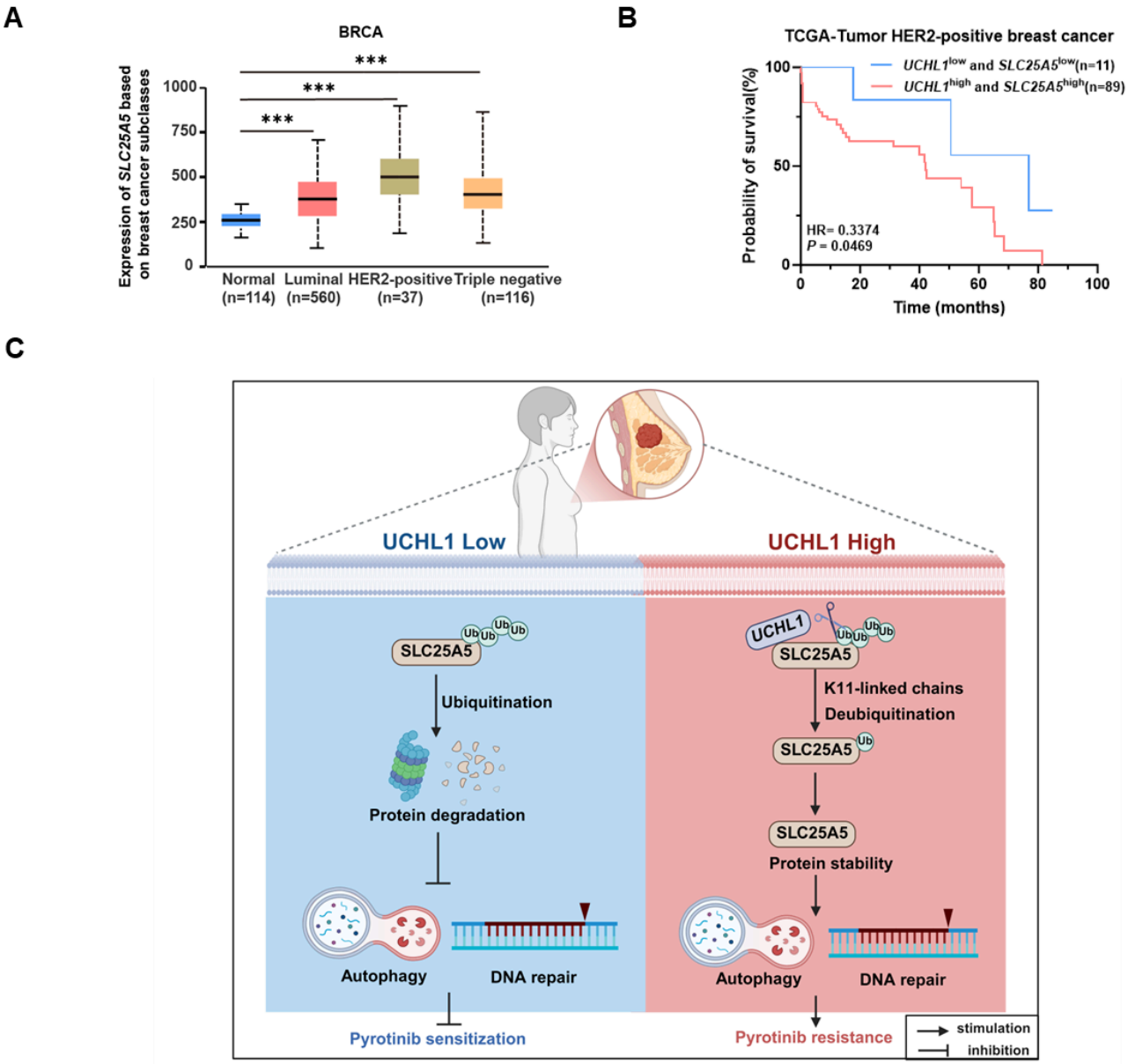


Figure 6

The prognostic significance of the UCHL1-SLC25A5 axis in HER2-positive breast cancer. A Box plot showing the mRNA expression levels of SLC25A5 in normal breast tissues (n=114), Luminal subtype (n=560), HER2-positive subtype (n=37), and triple-negative breast cancer (TNBC, n=116) from the TCGA dataset. Error bars represent Mean ± SEM. **B** Kaplan-Meier survival curves for overall survival stratified by combined expression status of UCHL1 and SLC25A5 in the TCGA HER2-positive breast cancer cohort.

Patients were divided into two subgroups: UCHL1 low/SLC25A5 low (n=11) and UCHL1 high/SLC25A5 high (n=89). HR = 0.3374, *P* = 0.0469. **C** Schematic diagram illustrating the molecular mechanism by which UCHL1 drives pyrotinib resistance in HER2-positive breast cancer. $^{***}P < 0.001$.

Supplementary Files

This is a list of supplementary files associated with this preprint. Click to download.

- Blots.pdf
- Supplementaryfigures.docx
- Highlights.docx
- Supplementtables.docx